NeuroImage 326 (2026) 121696

Contents lists available at ScienceDirect

NeuroImage

journal homepage: www.elsevier.com/locate/ynimg

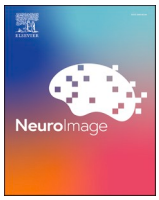

Organizational principles of the cerebral cortex predict symptoms progression in the Alzheimer's disease spectrum

Arianna Menardi [a,b,*], Beatrice La Rocca [c], Ceren Saglam [c], Francesco Alberti [d], Diego Cecchin [b,e], Annalena Venneri [f,g], Annachiara Cagnin [a,b], Antonino Vallesi [a,b], for the Alzheimer's Disease Neuroimaging Initiative (ADNI)[#]

[a] Department of Neuroscience, University of Padova, 35121, Padova, Italy
[b] Padova Neuroscience Center, University of Padova, 35121, Padova, Italy
[c] Department of General Psychology, University of Padova, 35131, Padova, Italy
[d] Integrative Neuroscience & Cognition Center, University of Paris, 75006, Paris, France
[e] Department of Medicine (DIMED), University Hospital of Padova, 35128, Padova, Italy
[f] Department of Medicine and Surgery, University of Parma, 43125, Parma, Italy
[g] Department of Neuroscience, University of Sheffield, S10 2TN, Sheffield, UK

ARTICLE INFO

Keywords:
Functional gradients
Default mode network
Alzheimer's disease
Topology
Morphology
Cognitive decline

ABSTRACT

Functional gradients offer a novel, synthetic and interpretable view of functional connectivity. By integrating gradients, graph theory, morpho-volumetric indices, amyloid status, and regional tau burden, we aim to understand how cognitive decline relates to functional and structural brain changes. We analyzed 279 participants from the Alzheimer's Disease Neuroimaging Initiative (ADNI) database with available functional, structural, and proteomic data at baseline and at 2-year follow-up, alongside detailed assessments of verbal memory abilities (encoding, retrieval and recall). Results at baseline revealed distinct patterns based on amyloid status and clinical severity. In individuals with positive amyloid status, increased functional dispersion of the Default Mode Network (DMN) correlated with poorer memory, while in individuals with negative status higher dispersion was associated with better performance. Notably, middle temporal regions exhibited connectivity profiles opposite to other DMN areas. We also observed that regions where gradients' dispersion predicted impaired memory performance showed preserved structural integrity but had a more widespread connectivity profile. Baseline dispersion predicted future memory decline, showing consistent patterns across positive and negative amyloid groups—higher dispersion was linked to faster memory decline, except in tau-rich regions like the temporal cortex, where it was advantageous. Furthermore, higher dispersion was associated with future tau buildup and morphological alterations. This study extends a previous investigation and evaluates the utility of a multimodal framework in tracking disrupted DMN activity as an early marker of reduced coherence in communication among brain regions, possibly having a predictive value for future progression of cognitive decline.

1. Introduction

Alzheimer's disease (AD) is the most common form of neurodegenerative disorder, posing significant burden on individuals (Lanctôt et al., 2024) and society (Nandi et al., 2022). As a complex and multifactorial pathology, AD can be described at different levels of abstraction. For instance, at a biological level, AD can be portrayed based on pathology-dependent spreading patterns of amyloid and phosphorylated tau deposits (Braak and Braak, 1991). At a neural level, it can be characterized in relation to its patterns of functional and structural alterations, while at the cognitive level, the patients' history of progressive memory, language, attention and executive dysfunctions guides clinical diagnostic criteria (Buckner et al., 2005; Tarawneh and Holtzman, 2012). To gain a more unitary view of the disease across all its levels,

* Corresponding author at: Department of Neuroscience, University of Padova, Padova, Italy.
E-mail address: arianna.menardi@unipd.it (A. Menardi).

[#] Data used in preparation of this article were obtained from the Alzheimer's Disease Neuroimaging Initiative (ADNI) database (adni.loni.usc.edu). As such, the investigators within the ADNI contributed to the design and implementation of ADNI and/or provided data but did not participate in analysis or writing of this report. A complete listing of ADNI investigators can be found at: http://adni.loni.usc.edu/wp-content/uploads/how_to_apply/ADNI_Acknowledgement_List.pdf.

https://doi.org/10.1016/j.neuroimage.2026.121696
Received 8 September 2025; Received in revised form 15 December 2025; Accepted 5 January 2026
Available online 5 January 2026

connectome-based approaches have gained interest as a possible method to address the interplay among the different aspects of AD pathophysiology, i.e. to understand the interdependent relationship between structural/functional alterations, amyloid/tau deposition and cognitive impairment (Yu et al., 2021). This has been particularly promoted by the biological framework of disease diagnosis and staging based on amyloid (A), pTau (T) and neurodegeneration (N) status (i.e., the ATN model) (Jack et al., 2018).

Within the ATN framework, the study of the Default Mode Network (DMN) has gained particular interest. The DMN is a resting state network consisting of the medial prefrontal cortex, posterior cingulate cortex, precuneus, and bilateral inferior parietal cortices, with a particular role in self-reference, social cognition, language, mind wandering and episodic memory (Menon, 2023), as well as higher order executive functions across the lifespan (Menardi et al., 2024). Although the DMN is not the only network affected by AD pathology, it is the most prominent given its early functional disruption linked to pathology onset and its greater overlap with the spatial distribution of proteinopathy, hypometabolism and atrophy spreading in this disease (Buckner et al., 2005; Hampton et al., 2020; Hu et al., 2022; Perovnik et al., 2023; Wang et al., 2024a; Zhou et al., 2022). Furthermore, several studies have linked the presence of amyloid and tau deposits to a progressive loss of connectivity in the affected regions, involving mainly, but not only, the DMN (for a review, see Yu et al., 2021).

In the field of connectivity, gradients' analyses are a recently proposed approach to investigate interindividual differences in functional differentiation (Bernhardt et al., 2022). In more detail, these are based on the definition of macroscale axes of functional organization in the cortex that have been observed across species (Margulies et al., 2016). The most informative gradients of functional organization extend from primary sensory regions to transmodal regions (first gradient), from somato-motor to visual regions (second gradient) and across task-positive and task-negative regions (third gradient) (Alberti et al., 2025; Hong et al., 2020; Margulies et al., 2016). This approach allows us to track changes in the hierarchy of cortical organization that might be linked to interindividual differences in behavior, proxies of pathology (Bernhardt et al., 2022), and changes in the differentiation between systems (Bethlehem et al., 2020). As in aging and pathology these latter changes might be expected to interest multiple gradients simultaneously, Bethlehem and colleagues introduced a measure of *dispersion* to investigate multi-dimensional differences in cortical organization (i.e., across multiple gradients' spaces at once) (Bethlehem et al., 2020). While in the original paper this measure was used to estimate changes in connectivity between- and within- functional communities, in the present study we applied it at the single parcel level to map the progressive functional differentiation of DMN nodes as a function of pathology that we expected to be captured by an increase in dispersion, and hypothesized that it would be associated with cognitive decline and clinical severity. While this approach is useful to chart the functional shifting of a brain region, it is less informative to describe how this change alters the role of that brain region in mediating information transfer within the brain. To address this limitation, we combined regional gradients' dispersion measures with topological indexes derived from a graph theory analysis, a highly generalizable mathematical approach useful to study complex networks (Bullmore and Bassett, 2011). When applied to the brain, networks are generated by modeling regions as nodes, and their functional (or structural) connections as edges (Rubinov and Sporns, 2010). Topological and geometric properties of the brain graph can then be investigated by a rich set of measures (Rubinov et al., 2009). For the purpose of this study, we relied on graph theory to determine if changes in gradients' dispersion could be explained by: i) an overall loss in the connectivity strength of DMN regions (nodal strength); ii) a shift of communication pathways towards different functional communities (participation coefficient); or iii) a loss in the overall centrality of DMN nodes in the brain network (betweenness centrality). While functional alterations might happen in the absence of biomarkers of atrophy or hypometabolism in prodromal AD stages (Palmqvist et al., 2017), more complex co-dependences are observed at later stages (Talwar et al., 2021).

In a recent study (Menardi et al., 2025), we described how morphological changes within the DMN (cortical thinning, gyrification and sulcal depth) are predictive of memory performance, highlighting the differential susceptibility of these measures to the individual amyloid status and degree of cerebral tau burden. The present study aims at expanding this earlier evidence by investigating DMN system failure from a functional perspective, particularly by leveraging on gradients analyses. This is motivated by the fact that examining functional alterations of the connectome—not just structural changes in its regions—is crucial, as these may serve as earlier biomarkers of pathology, preceding the neuronal loss detected by atrophic measures and helping to determine the temporal window during which disease-modifying interventions should be implemented (Yu et al., 2021). Only a small number of multimodal studies has simultaneously investigated the relationship between functional disconnection and structural alterations, and how this interaction is influenced by amyloid/tau deposits in predicting long-term cognitive decline in the same patients' population. In particular, no study has relied on regional dispersion values in the gradient space to characterize progressive network disaggregation, nor has any work investigated how this relates to regional structural and topological changes. As for the use of gradient analysis, prior investigations have shown a link between cognitive decline and gradients' variance reduction both at the whole brain level (Hu et al., 2022), and in selective regions (i.e., the medial parietal cortex) (Veréb et al., 2023), as a function of gene expression (Wang et al., 2024b) and tau pathology (Ottoy et al., 2024). To our knowledge, only one prior study has investigated dispersion measures in AD (He et al., 2023). However, dispersion measures were used to characterize the global loss of functional differentiation in whole-brain connectivity patterns, without assessing its association with amyloid and tau burden or structural morphological alterations.

2. Materials and methods

2.1. Participants

Data used in the preparation of this article were obtained from the Alzheimer's Disease Neuroimaging Initiative (ADNI) database (adni.loni.usc.edu). The ADNI was launched in 2003 as a public-private partnership, led by Principal Investigator Michael W. Weiner, MD. The original goal of ADNI was to test whether serial magnetic resonance imaging (MRI), positron emission tomography (PET), other biological markers, and clinical and neuropsychological assessment can be combined to measure the progression of mild cognitive impairment (MCI) and early Alzheimer's disease (AD). The current goals include validating biomarkers for clinical trials, improving the generalizability of ADNI data by increasing diversity in the participant cohort, and to provide data concerning the diagnosis and progression of Alzheimer's disease to the scientific community. For up-to-date information, see adni.loni.usc.edu. Informed consent was obtained from all participants enrolled by the ADNI consortium prior to participating in data collection, in accordance with the Declaration of Helsinki (https://adni.loni.usc.edu/help-faqs/adni-documentation/).

The sample of participants is the same as described in (Menardi et al., 2025). Briefly, we initially considered 575 participants from the 3rd cohort of ADNI (healthy controls-HC = 183, MCI = 321, AD = 71) for which structural, functional and cognitive variables were available for at least 2 timepoints: baseline and 2 years follow-up (Y2). Some participants (n = 13 MCI; n = 5 AD) were later excluded due to high motion inside the scanner (framewise displacement greater than 0.5 mm). Our participants' group was then further down sampled to retain only participants with available Amyloid (A, status is defined as positive or negative ±) and Tau PET data acquired within 6 months from the MRI

acquisition. This resulted in $n = 129$ $A+$ ($M = 74.7 \pm 9.8$ years of age) and $n = 150$ A- ($M = 72.1 \pm 7.8$ years of age) at baseline and $n = 78$ $A+$ and $n = 98$ A- at Y2. Information on Discontinuation and Withdrawal of patients is available on the ADNI website (https://adni.loni.usc.edu/).

2.2. Cognitive evaluation

In this study, the Mini Mental State Examination (MMSE) and the Embic Digital Cognitive Biomarker scale (EMBIC-DCB) were used as measures of cognitive functioning. In detail, MMSE scores were used as estimates of individual global cognitive performance to infer the level of clinical severity of the patients. Indeed, rather than stratifying participants according to diagnostic status (HC, MCI and AD), we used their MMSE scores as a continuous proxy of disease severity in the models (see Statistical Analyses paragraph). Additionally, the EMBIC-DCB scale was chosen to monitor memory impairments, given its reported higher sensitivity to early memory failure, enabled by the use of a Bayesian cognitive hierarchical model applied at the single item level across multiple word-recall lists to derive encoding, retrieval and recall efficiency estimates (for a more in depth explanation of the scale refer to Bruno et al., 2024 and Lee et al., 2020) and the original ADNI documentation). EMBIC-DCB scores are available for up to 10 years of follow-up but to retain enough statistical power, we focused on baseline and year 2 measures (Y2).

2.3. Neuroimaging data

2.3.1. Structural MRI

Structural MRI data were analyzed as described in (Menardi et al., 2025). Briefly, preprocessing of the structural images involved brain extraction and bias field correction by means of ANTs (Advanced Normalization Tools) (antBrainExtraction and N4BiasFieldCorrection functions) (Tustison et al., 2021). The FSL FAST algorithm was used to perform tissue segmentation (Zhang et al., 2001), followed by MNI normalization by means of ANTs (Tustison et al., 2021). Finally, regional structural measures of cortical thickness, gyrification and sulcal depth were extracted by means of CAT12 (Gaser et al., 2024). Thickness and gyrification indexes were extracted following a smoothing of 15 mm and 20 mm FWHM filters, respectively, following CAT software recommendations.

2.3.2. Functional MRI

fMRI data were acquired on a 3T Siemens PRISMA scanner (TR = 3000 ms, TE = 30 ms, flip angle = 90°, number of volumes = 197, voxel size (isotropic) = 3.4 mm, 64×64×48 matrix, total acquisition time = 15 min). Preprocessing of the functional images involved slice timing correction, motion correction with mcflirt (Jenkinson et al., 2002), distortion correction based on field maps acquisition and bias field correction with ANTS (Tustison et al., 2021). FLIRT was used to coregister each participant's functional and anatomical volume using 7 degrees of freedom and a boundary-based constriction relying on each individual white matter mask (Greve and Fischl, 2009). CompCor (Components based Noise Correction) (Behzadi et al., 2007) and ART (Artifact Rejection Toolbox) functions were further applied to perform scrubbing and remove additional noise components following the CONN denoising pipelines (Nieto-Castanon, 2020). Spatial smoothing with a gaussian kernel with a full width at half maximum of 8 mm was applied. Finally, the Schaefer 400 functional parcellation (Schaefer et al., 2018) was applied to individual EPI space by using the inverse of the transformation matrices of structural normalization and structural-functional coregistration.

2.3.2.1. Graph Theory measures. The individual functional connectivity matrix was constructed based on the Pearson's correlation across the timeseries of all 400 parcels. Correlational values inside the matrix underwent normalization (Fisher z-score) and strict multiple comparison correction by retaining only the 10 % of the strongest ties within the matrix. This stringent approach minimized risk of false positive connections that might result in artefactual graph theory measures, while easing the comparison with gradients-derived connectivity measures for which a similar threshold is applied prior to their computation (see next paragraph). We have applied this approach in another prior work by some of the authors (Alberti et al., 2025).

In this study, we focused on three nodal graph theory measures that were computed in Matlab 2023a (MathWorks, Natick, MA) relying on the available functions of the Brain Connectivity Toolbox (https://sites.google.com/site/bctnet/) (Rubinov et al., 2009). The following measures were chosen because they highlight the role of DMN regions in mediating information transfer within and between network(s) (Rubinov and Sporns, 2010):

- Nodal strength (NS): measured as the sum of the weights of the edges connecting to one node. Nodes with higher NS will hence benefit from strongest functional connectivity;
- Participation Coefficient (PC): a measure of diversity of intermodular connections, such as that nodes with high PC values will tend to share edges with nodes belonging to different modules;
- Betweenness Centrality (BC): measured as the fraction of shortest paths going through a given node. A node with high BC, therefore, will be central in the network as many short paths pass through it.

2.3.2.2. Functional Gradients. Gradients were computed using the BrainSpace Toolbox (Vos de Wael et al., 2020) starting from the individual functional connectivity matrix that was thresholded to retain only the top 10 % of the connections (number of edges retained = 16, 000). This level of sparsity reflects a default parameter in Gradient Computation that minimizes risk of false positive connections that could possibly alter truthful gradients' extraction. In this study, we opted to extract gradients using a normalized angle kernel and a diffusion embedding approach, resulting in an initial definition of 10 components. This methodological choice ensured that gradients' order remained stable across participants compared with using other kernels and/or dimensionality reduction techniques. This represents a prerequisite for the alignment procedure, described next. Following the examination of eigenvalues, we focused on the first three gradients, as these explained most variance in the data (see Fig. 1A). To ensure gradients comparability across individuals, they were aligned to the average gradient of the healthy controls through Procrustes analysis.

Finally, we computed a measure of regional gradients' *dispersion* that represents the Euclidean distance of the gradients' values in every DMN parcel from the median gradients' values of their network (Bethlehem et al., 2020). The higher the dispersion of one parcel, the more the parcel has a connectivity profile that is functionally different from that of the network it should be part of. In other words, dispersion can be considered a measure of decoupling.

2.3.3. PET Imaging

Dichotomization of amyloid status (±) was derived from the ADNI repository (ADNI_UCBerkeley_AmyloidPET), which applies a cutoff of 1.11 standard uptake value ratios (SUVR) for *florbetapir* and 1.08 SUVR for *florbetaben*. For Tau deposition, we included only participants who had undergone Tau PET scans (ADNI_UCBerkeley_TauPET) with the same tracer (flortaucipir). Tau PET SUVR are already provided corrected for partial volume effects and intensity normalized using the inferior cerebellar grey matter as reference region. However, because tau SUVR values are provided according to the Desikan-Killiany Atlas 40, we carried out a vertex-to-vertex correspondence analysis between the Schaefer and Desikan-Killiany atlases at the cortical surface level, thereby mapping tau deposits to Schaefer parcels based on their overlap with Desikan-Killiany regions as described in Menardi et al., 2025.

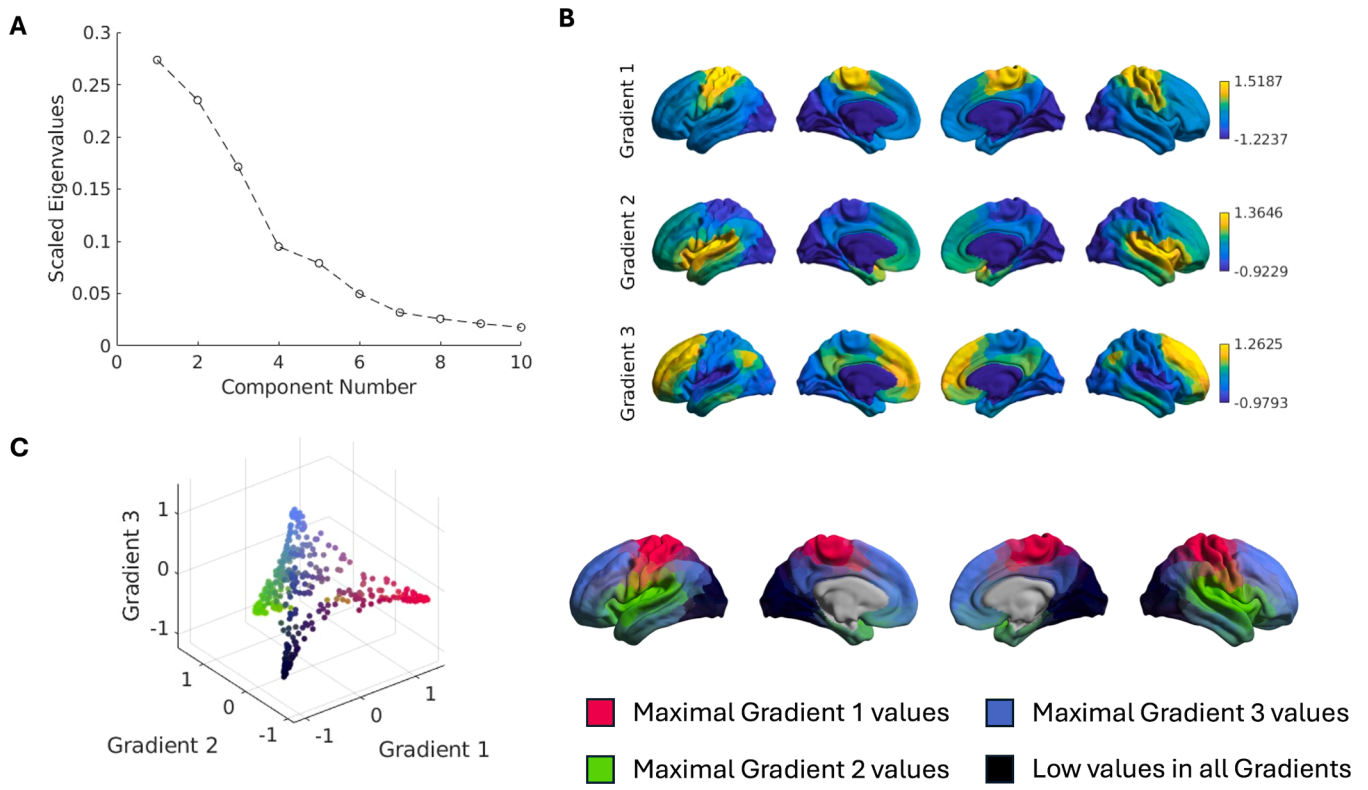

Fig. 1. Functional Gradients. A. Eigenvalues plot of the first 10 components. Higher eigenvalues indicate more important components in explaining functional connectivity patterns. **B.** Order of functional connectivity gradients after Procrustes analysis, resulting in the visual-sensorimotor (gradient 1), sensory-insular (gradient 2) and sensory-DMN (gradient 3) connectivity axis. **C.** Regional gradients values presented in 3D space, as well as on the cortical surface.

Measures of tau deposition were used as a continuous variable in our analyses.

For both amyloid and tau imaging, only participants who had a PET scan within six months from their MRI acquisition were included, ensuring temporal alignment between modalities and reducing the likelihood that biological changes over longer time intervals would confound interpretations (Schuff et al., 2009). The distribution of the average DMN thickness and tau SUVR values, as well as their joint distribution, for *A*+ and A- individuals is shown in Supplementary Figure 1.

2.4. Statistical Analyses

Statistical analyses were run in Matlab 2023a (The Mathworks, Inc., Natick, MA, United States). We analyzed *A*+ and A- individuals separately in consideration of the impact of amyloid positivity in shaping functional connectivity alterations (Yu et al., 2021). First, one-way Analysis of Variance (ANOVA) models were used to check for significant differences in the mean DMN dispersion values across participant groups (HC, MCI and AD). Then, multiple linear regression analyses were used to test if gradients' dispersion, graph theory (nodal strength, participation coefficient, betweenness centrality) and structural measures (gyrification, thickness, sulcal depth) could predict EMBIC-DCB performance. We followed the same analytical approach as described in our earlier work (Menardi et al., 2025). However, while in that study we had only focused on the predictive power of DMN morphological measures, in this study we extended our investigation to include more comprehensive, multidomain analyses of both structural *and* functional indexes of DMN integrity, or lack thereof. In brief, encoding (N1, N2, N3, N4), retrieval (R1, R2, R3) and recall (M1, M2, M3) scores from the original EMBIC-DCB scale were averaged into single measures (N, R, M), to minimize risk of multiple comparisons. Individuals' age, MMSE scores, years of education, framewise displacement and regional tau burden were included as covariates in the analyses, together with their interaction with the predictors. This represents an attempt to study the association between AD pathology and cognitive decline within the ATN framework. Rather than carrying out our analyses using models based on rigidly defined diagnostic groups (e.g. HC, MCI and AD), we built models in which indices of amyloid status (A), cerebral tau accumulation (T) and structural alteration (N) were considered. The significant interactions among such predictors were then examined to characterize the association between pathological aging and cognitive performance along a biological continuum. Multicollinearity in the models was checked by ensuring that the variance inflation factor remained ~1. Furthermore, outliers were removed based on the models' residuals, as determined by a cut-off of ±3 scaled absolute deviations from the median (average $n = 3$ participants). To meet the objectives of this study, we were interested in assessing the presence of significant interactions between regional dispersion and MMSE. For those significant nodes, we also aimed to determine: i) the relationship between regional dispersion and tau deposits in A+ and A- groups; ii) the interaction between regional dispersion and graph theory measures in A+ and A- groups; iii) and the interaction between regional dispersion and structural measures in A+ and A- groups. To control for the risk of multiple comparisons, only models surviving FDR ($p = 0.05$) correction were considered.

Finally, we conducted Pearson's correlation analyses to test whether baseline regional dispersions would predict future tau deposits and atrophy within the same regions. A methodological workflow representing the main data, variables of interest and analysis plan is schematized in Fig. 2.

3. Results

3.1. DMN dispersion as predictor of baseline memory performance

In line with the known involvement of the DMN in AD, ANOVA revealed a significant increase in dispersion values as a function of

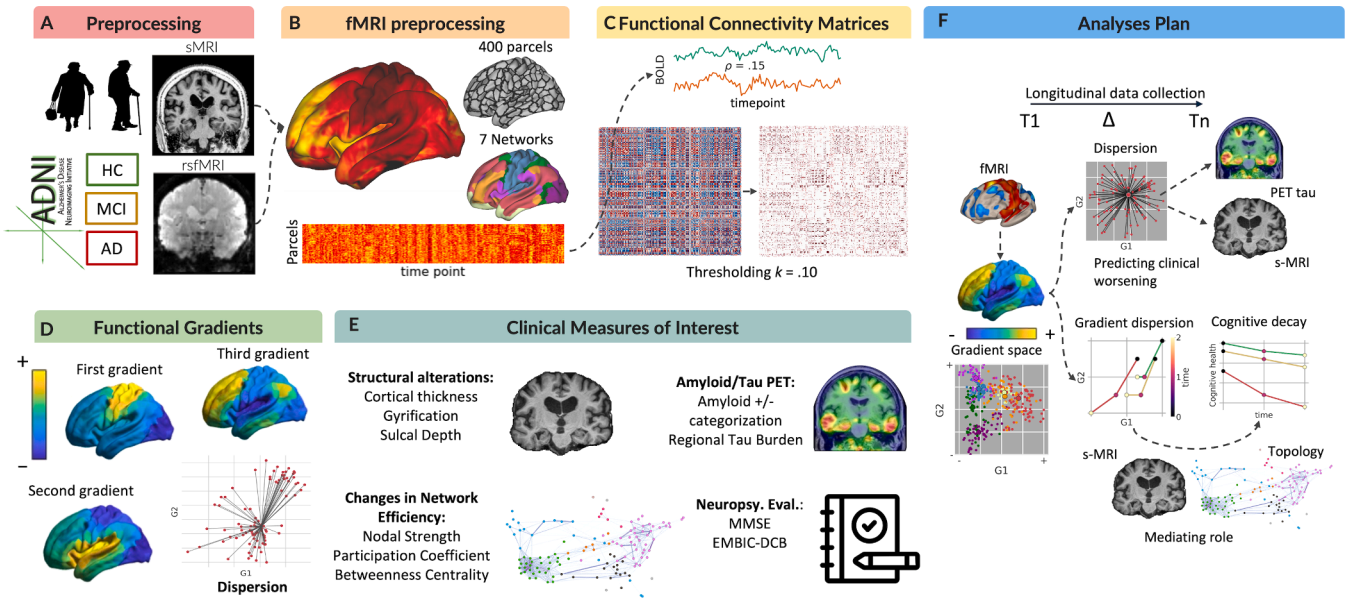

Fig.2. Methodological workflow. Structural and functional data available at baseline and at 2-year follow-up were retrieved from the ADNI dataset (**A**). The Schaefer functional parcellation was used to divide the cerebral cortex in 400 regions of interests and seven resting state networks (**B**). Functional connectivity matrices were derived as the product of the Pearson's correlation between the BOLD signal of each pair of regions and further thresholded to retain only the top 10 % of connections (**C**). Functional gradients representing the organizational principles of the cerebral cortex were computed, together with measure of regional dispersion, describing the functional differentiation of each DMN parcel in respect to the network's median activity profile (**D**). Regional dispersion was put in relation with several clinical variables of interest (**E**) and used to predict longitudinal cognitive decline, proteinopathy and atrophy.

pathology ($F_{(2,554)}$= 4.93, p = 0.007), with post hoc analyses discriminating HC (M = 43.15±14.3) from MCI (M = 46.7 ± 15.4, p = 0.038) and AD (M = 49.3 ± 18.3, p = 0.014) patients, but not between MCI and AD (p = 0.41). Furthermore, lower MMSE scores were associated with higher DMN dispersion (r = −0.14, p = 0.0013). To understand better the association between regional dispersion and cognitive decline, multiple linear regression models were run, separately for A+ and A- individuals. All models were corrected to minimize risk of multiple comparisons using FDR ($p < 0.05$).

Interestingly, we observed marked opposite patterns in the relationship between DMN dispersion and memory performance in the A+ and A- groups, with the regions emerging as significant mostly located in the left hemisphere in both groups. This appears in line with the verbal nature of the stimuli used to assess memory performance.

In the A+ group, we observed that several regions emerged as significant predictors of encoding (number of significant regions = 11), retrieval (number of significant regions = 4) and recall (number of significant regions = 14) as a function of clinical severity (MMSE score). In more detail, increased dispersion of frontal and posterior parietal regions (left dorsomedial prefrontal cortex - DMPFC, left dorsolateral prefrontal cortex - DLPFC and left inferior parietal lobule - IPL) was associated with poorer encoding and recall performance (see Fig. 3A), while regions in the bilateral middle temporal gyrus (MTG) showed an opposite pattern across conditions, with higher functional differentiation being associated with better performance.

In the A- group, we prevalently observed positive relationships between the degree of functional differentiation of DMN regions and performance at encoding (number of significant regions = 16), retrieval (number of significant regions = 8) and recall (number of significant regions =16). More specifically, these regions were located in the DLPFC, DMPFC, inferior temporal gyrus, anterior and posterior cingulate regions (ACC, PCC), mainly in the left hemisphere (see Fig. 3A). As noted for the A+ group, the left MTG also presented an inverted pattern, with higher dispersion being associated with worse encoding and recall performance.

Overall, these results suggest that greater functional dispersion of the DMN is associated with worse memory performance in the pathological group (A+), whereas the opposite is true in the non-pathological sample (A-), whose performance was facilitated by a certain degree of functional differentiation. Bilateral temporal regions present a pattern of their own, opposite to the rest of the DMN.

Models' statistics are available in Supplementary Tables 1 and 2 of the Supplementary Materials.

3.2. Baseline DMN dispersion and tau pathology

Given recent evidence on the connectome-based spread of tau pathology (Franzmeier et al., 2020), we decided to look specifically at the interaction between DMN regional dispersion and tau deposits as a function of amyloid status.

In the A+ population, we observed a significant difference in the average amount of tau deposits ($F_{(2,126)}$= 7.61, p = 0.0008), with significantly higher values in AD patients (M_{SUVR}= 1.82±1.04) than in MCI (M_{SUVR}= 1.45±0.58, p = 0.003) and HC (M_{SUVR}= 1.67±0.14, p = 0.04) individuals. On the other hand, in the A- population, we observed no difference in the accumulation of tau between HC and MCI individuals ($t_{(144)}$= 1.06, p = 0.289). Furthermore, MMSE scores were negatively associated with average DMN tau deposits in the A+ population (r = −0.50, $p < 0.0001$), but not in the A- group (r = −0.15, p = 0.076). Finally, age was negatively associated with tau deposits in the A+ group (r = −0.27, p = 0.001) but positively associated in the A- group (r = 0.28, p = 0.0007). This pattern confirms that tau accumulation is linked to younger age in the presence of amyloid pathology (Jack et al., 2020; Whitwell et al., 2019), while in individuals with a negative amyloid status, accumulation of tau pathology seems to increase with advancing age, a condition known as primary age-related tauopathy (PART) (Crary et al., 2014).

In terms of the interaction between regional dispersion and tau deposits as predictor of memory performance, we also observed opposite patterns between A+ and A- individuals (see Fig. 4). In the A+ group, significant negative interactions were mainly observed in the left MTG and bilateral ACC. This finding suggests that the greater the amount of tau deposits within these regions, the more their functional dispersion is associated with poorer memory performance. Interestingly, an

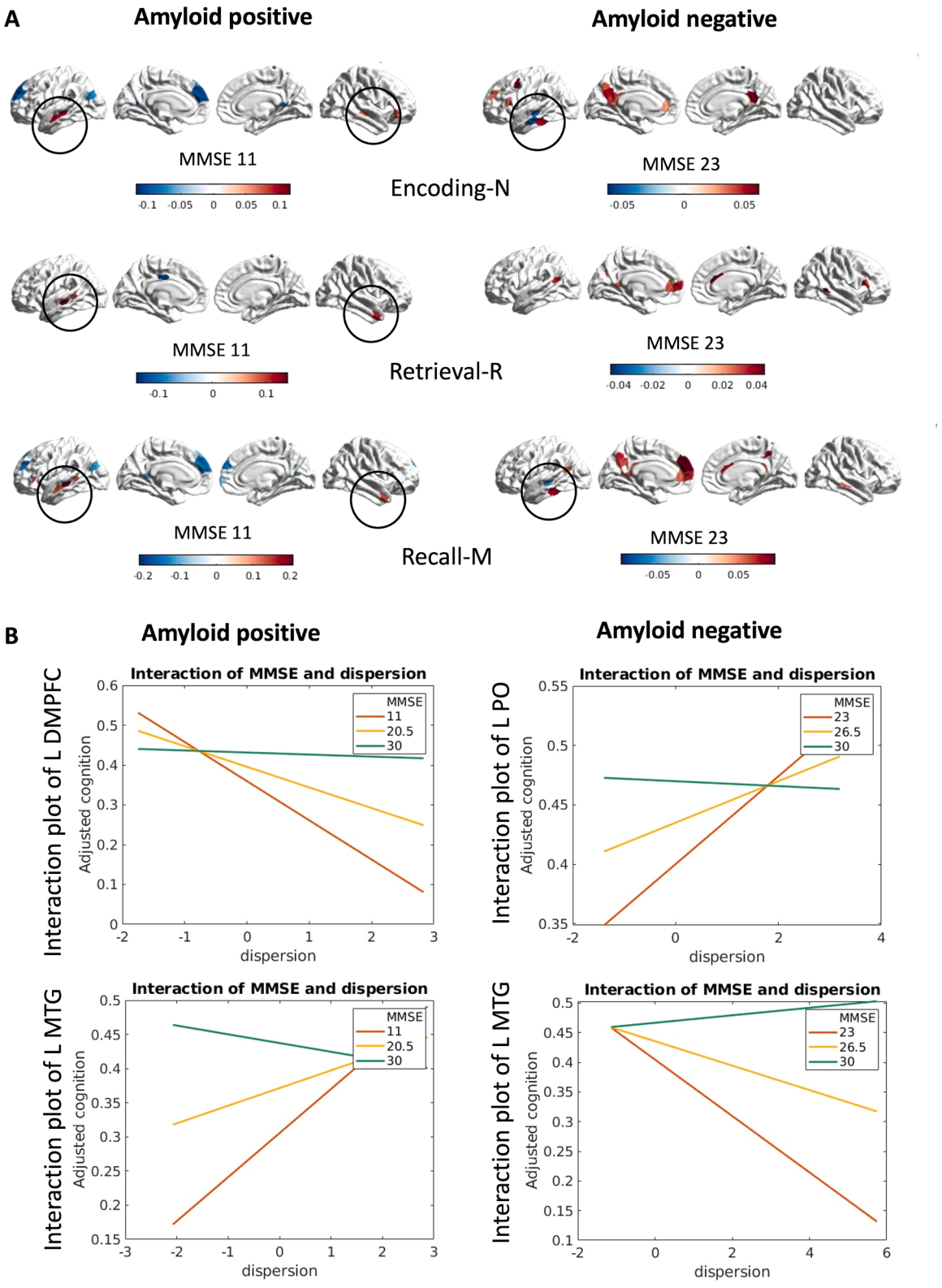

Fig. 3. Surface plots of significant dispersion by MMSE interactions. Nodes presenting significant interactions between their level of dispersion and patients' MMSE scores are plotted on the surface for both the A+ and A- populations (**A**). The color code of the regions plotted on the surface represents the slope of the interaction (i.e., blue regions indicate a negative interaction between dispersion and MMSE scores, whereas red colored regions indicate a positive pattern). Interaction plots of few representative regions for which dispersion measures were observed to interact significantly with patients' MMSE in predicting encoding performance are shown (**B**). Stronger relationships are present for more severe patients and, for both populations, MTG shows opposite interaction patterns than the rest of the significant DMN regions (marked by a circle).

DMPFC = dorsomedial prefrontal cortex; *L* = left hemisphere; MMSE = Mini Mental State Examination; MTG = middle temporal gyrus; PO = pars opercularis.

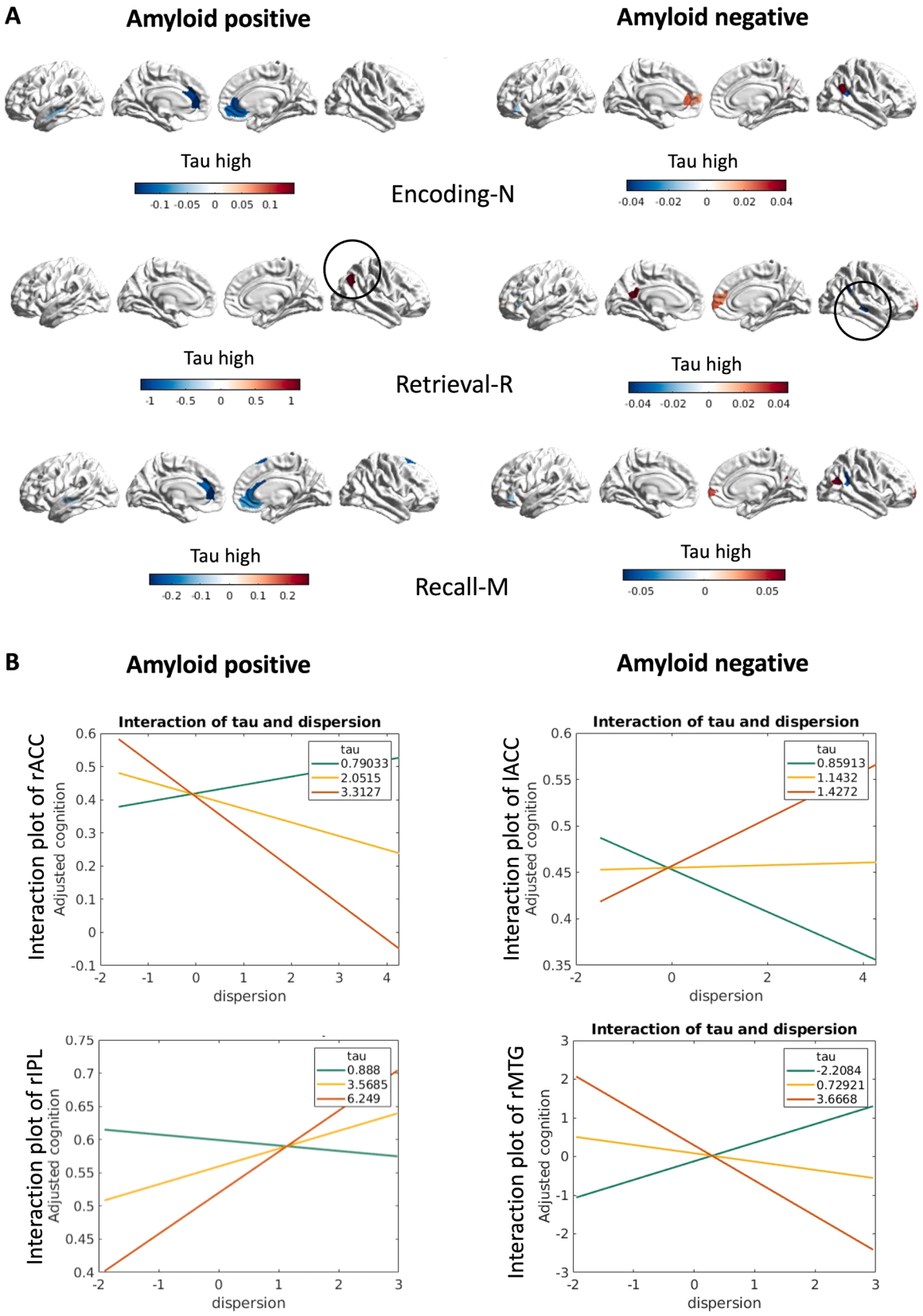

Fig. 4. Surface plots of significant dispersion by tau interactions. Nodes presenting significant interactions between their level of dispersion and patients' tau deposits are plotted on the surface for both the A+ and A- populations (**A**). The color code of the regions plotted on the surface represents the slope of the interaction (i.e., blue regions present a negative interaction between dispersion and tau deposits, whereas red colored regions present the opposite pattern). Regions showing inverted patterns compared with the other DMN nodes are marked with a circle. Interaction plots of few representative regions are shown (**B**).
ACC = anterior cingulate cortex, IPL = inferior parietal lobule, *l* = left, MTG = middle temporal gyrus, *r* = right.

exception to this pattern is represented by the right IPL that shows a positive relationship between its degree of dispersion and recall abilities (see Fig. 4A, marked by a circle). When there is high regional tau load within this region, its functional differentiation appears to facilitate better recall performance. Models' statistics are available in Supplementary Table 1 of the Supplementary Materials.

Even though regional tau burden was significantly lower in A- individuals than in A+ individuals ($t_{(180)}= -22.5$, $p < 0.0001$), we also observed few significant interactions also in this group. In detail, A- individuals with higher tau deposits (SUVR≥1.4) presented marked positive associations between dispersion values and encoding, retrieval and recall performance. These interactions mainly involved the left ACC (for encoding), the left PCC/right ACC (for retrieval) and the right IPL (for both encoding and recall). As the DMN can be divided into different functional subsystems that underlie a wide spectrum of cognitive functions (Mancuso et al., 2022), a certain degree of heterogeneity in the activity of its regions might have beneficial effects on the behavioral performance of healthy individuals.

Of note, a small portion of the right MTG was the only region displaying a negative association with retrieval abilities (see Fig. 4A, marked by a circle). This means that higher functional dispersion and tau burden in this region result in greater retrieval impairment in A- individuals.

Models' statistics are available in Supplementary Table 2 of the Supplementary Materials.

3.3. Association between baseline dispersion, topology and structural alterations

The aim of this study was to establish if changes in regional dispersion values are accompanied by specific topology and/or structural alterations.

Only for a few regions, we observed that in A+ individuals with low MMSE scores the negative relationship between dispersion and encoding performance (see previous paragraph) was also accompanied by a negative relationship between thickness and gyrification with encoding, retrieval and recall performance scores. This finding suggests that the regions in which altered functional patterns are most predictive of impaired memory performance are also those with better preserved structural integrity. In predicting encoding and recall, most negative interactions with thickness and gyrification appeared to involve the DMPFC, DLPFC, IPL and MTG in the left hemisphere (see Supplementary Figure 2A and C). Only two regions emerged as predictive of retrieval performance (see Supplementary Figure 2B): a small portion of the left MTG presented the same negative pattern described above, whereas the sulcal depth of a region within the posterior cingulate cortex showed a positive association with retrieval performance. Given that sulcal depth decreases as a function of pathology and neurodegeneration (Im et al., 2008), the observed pattern confirms that a more preserved morphology of the cingulate cortex is more likely to be associated with better retrieval abilities.

From a topological perspective, we observed that most regions presented a negative association between nodal strength and memory performance, especially recall, whilst displaying a positive association with participation coefficient (PC) values. These regions included the left DMPFC, left MTG, left IPL and right DMPFC (see Supplementary Figure 2C). This pattern suggests that regions for which functional dispersion was associated with better memory performance also presented lower nodal strength (NS) but higher PC values. In individuals with an A+ status but more spared memory abilities, DMN connectivity strength appeared hence diminished but more widely distributed. The only exception was a small region in the precuneus, for which encoding performance was negatively associated with PC, but positively with NS (see Supplementary Figure 2A). This finding indicates that, for this region, better encoding performance is associated with greater within DMN connectivity of the precuneus.

Models' statistics are available in Supplementary Table 1 of the Supplementary Materials.

As for A- individuals, we observed that alterations in DMN dispersion were accompanied by a more complex profile of structural and topological changes compared with A+ participants. For instance, this patients' group also presented a negative association between thickness and memory performance, as observed in the A+ group, although it remained limited to the left ACC in predicting encoding/recall. Contrary to the A+ group, the gyrification index in the A- group was positively associated with encoding/recall performance, but the only significant region was the left precuneus (see Supplementary Figure 3A and C). Similar to the A+ group, sulcal depth measures showed both positive (left DLPFC and PCC) and negative (left precuneus, anterior CC and MTG) relationships, especially in predicting encoding (see Supplementary figure 3A). We can, therefore, conclude that in A- individuals with low MMSE performance, regions with higher dispersion that is predictive of better memory performance present lower thickness —a typical neurodegenerative marker— but preserved gyrification.

From a topological perspective, alterations in the left MTG appeared to play a role in predicting encoding, with higher participation coefficient and lower centrality of this region being associated with more successful performance. Finally, higher centrality of the bilateral precunei, left MPFC and right MTG appeared to facilitate recall performance. Overall, the more preserved the functional connectivity profile of several DMN regions, in terms of strength and centrality in within-network communication pathways, the more proficient the memory performance of the individual. As observed when describing dispersion patterns, the left MTG interestingly shows an inverted pattern compared with other DMN nodes.

Models' statistics are available in Supplementary Table 2 of the Supplementary Materials.

3.4. DMN dispersion as predictor of memory performance at 2 years follow up

For both A+ and A- individuals, baseline dispersion values of several DMN regions remained predictive of future cognitive decline at 2 years follow up (see Fig. 5).

Differently from what was observed at baseline, A+ and A- individuals showed the same patterns, albeit involving slightly different regions. For instance, all individuals with low MMSE scores showed a negative association between their baseline dispersion values and future cognitive decline, indicating a faster decline especially of retrieval and recall abilities. In A+ individuals, these patterns involved the bilateral PCC and bilateral MTG (see Fig. 5C), whereas A- individuals showed significant patterns in the left IFC, bilateral ACC and left MTG (see Fig. 5E). For both A- and A+ groups, less severely impaired participants (high MMSE scores) showed exactly opposite patterns compared with the low MMSE performers. For them, functional differentiation of these DMN regions was associated with better cognitive maintenance (positive relationship). Of note, the effects in higher MMSE performers were not as marked as in the low performers, as evidenced by the difference in magnitude of the color bar (see Fig. 5). Furthermore, in the A- group, MTG regions presented again inverted patterns compared with the rest of the significant DMN regions (see Fig. 5E). In this case, functional differentiation of the left MTG in low MMSE performers was positively associated with retrieval abilities at 2 years follow-up.

For both A+ and A- individuals, the interaction between baseline dispersion values and regional tau burden also emerged as significant in predicting future encoding, retrieval and recall abilities. For both groups, if a region at baseline presented high levels of tau burden, its functional differentiation from the rest of the DMN was positively associated with future memory performance. Conversely, regions displaying low levels of tau burden at baseline benefitted from less dispersion. These patterns were observed for small regions within the left IFC and left PCC for encoding and retrieval/recall in A+ participants

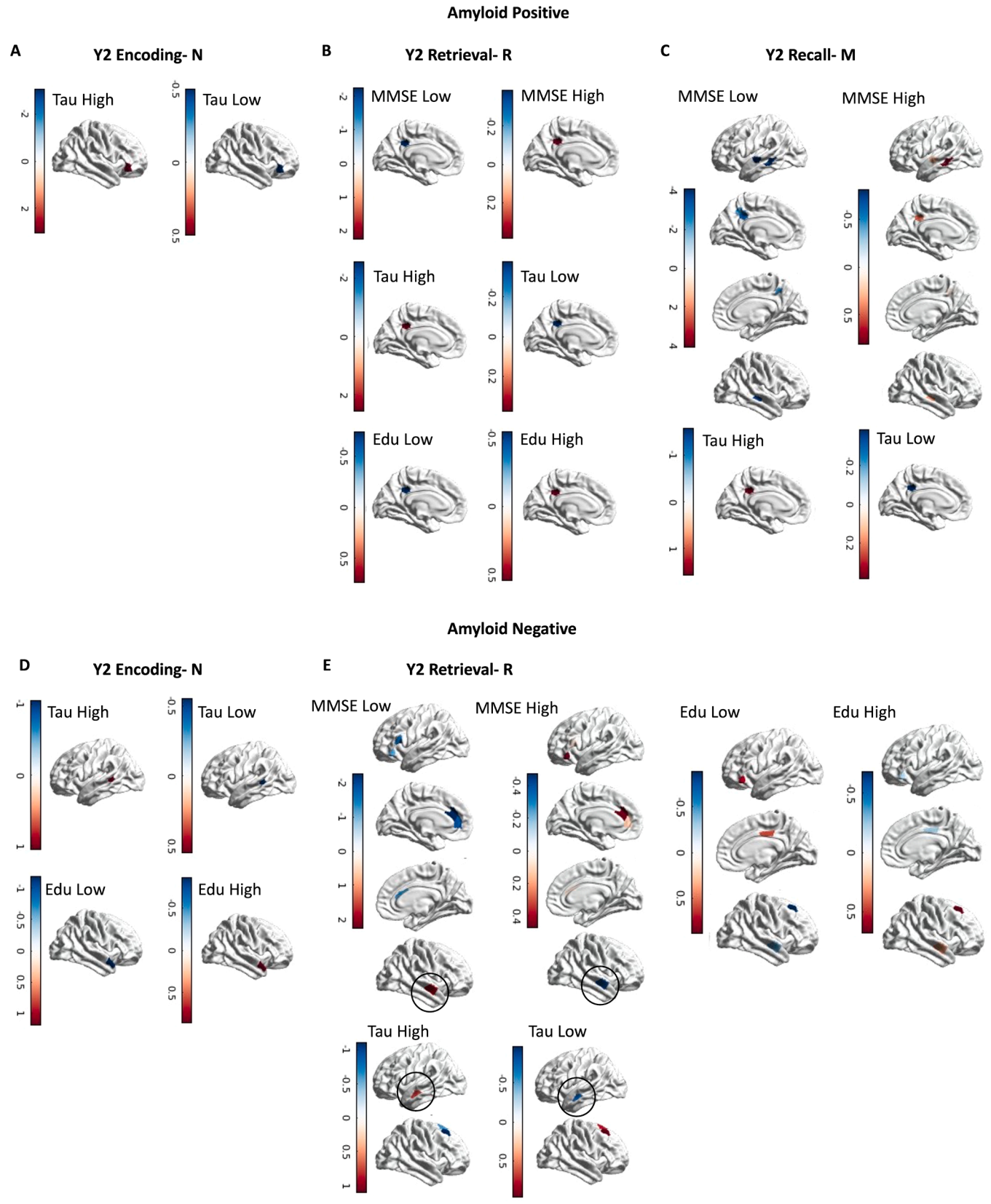

Fig. 5. Surface plots of DMN regions predictive of future memory performance. Nodes presenting significant interactions between their level of dispersion and patients' MMSE, tau deposits and level of education are plotted on the surface for both the A+ (**A, B, C**) and A- populations (**D, E**). The color code of the regions plotted on the surface represents the slope of the interaction (i.e., blue regions are those with a negative interaction between dispersion and future memory performance, whereas red colored regions show the opposite pattern). Regions showing inverted patterns compared with the other DMN nodes are marked with a circle. Edu = education (measures in years), MMSE = Mini Mental State Examination, Tau = Standard Uptake Values of regional Tau.

(see Figure5A, B and C), and for the left MTG and right DLPFC for A- individuals (see Fig. 5D and E). Models' statistics are available in Supplementary Tables 3 and 4 of the Supplementary Materials.

Finally, we checked for the potential protective role of higher education on future memory decline and its impact on DMN dispersion values. In both groups, individuals with higher education benefited from higher dispersion (suggesting greater functional differentiation) in few DMN regions, and this was associated with better memory proficiency at 2 years follow up. This pattern was limited to the left PCC in A+ individuals in predicting retrieval, whereas it extended to the right MTG and right DLPFC in A- subjects. Individuals with lower education presented opposite patterns (see Fig. 5B, D and E). The association between dispersion and education for baseline memory performance is instead discussed in the Supplementary Materials (see Supplementary Materials and Supplementary Figure 4).

3.5. Baseline dispersion values as predictors of future tau accumulation

Pearson's linear correlation analyses revealed that baseline dispersion values in several DMN regions were meaningfully associated with future tau deposits, measured as the slope in the increase of tau burden at Y2 compared with baseline. More positive values are, therefore, indicative of faster accumulation rates. In the A+, these regions included the right MTG ($r = 0.3$, $p = 0.03$) and the right PCC ($r = 0.28$, $p = 0.04$) (see Fig. 6A). In the A- group, the left ACC ($r = 0.4$, $p = 0.02$), left precuneus ($r = 0.48$, $p = 0.02$), right orbitofrontal cortex (OFC) ($r = 0.42$, $p = 0.04$), right ACC ($r = 0.47$, $p = 0.02$) emerged as significant (see Fig. 6B).

However, none of these correlations survived FDR correction for multiple comparisons, possibly due to the small number of participants in the 2 year follow-up group (A+: $n = 49$; A-: $n = 22$).

3.6. Baseline dispersion values as predictors of future atrophy

Pearson's linear correlation analyses revealed that baseline dispersion values in several DMN regions were meaningfully associated with future atrophy of the same regions, measured as the slope in the increase of atrophy at Y2 compared with baseline. More negative values are indicative of faster atrophy rates. For both A+ and A- individuals, higher dispersion values at baseline were generally associated with significant decrease in thickness, but increased gyrification at Y2. Results for sulcal depth showed mixed patterns.

In A+ individuals (see Fig. 7A), the dispersion values of the left MTG ($r = -0.22$, $p = 0.03$), left ACC ($r = -0.3$, $p = 0.003$), left DLPFC ($r = -0.22$, $p = 0.03$), and two regions of the right IPL ($r = 0.23$, $p = 0.02$; $r = -0.26$, $p = 0.01$) were predictive of future changes in thickness. Dispersion values in the lDLPFC ($r = 0.21$, $p = 0.04$), two regions in the rIFC, ($r = 0.22$, $p = 0.03$; $r = 0.21$, $p = 0.04$) and rPCC ($r = 0.25$, $p = 0.01$) were predictive of their future increase in gyrification. Finally, higher dispersion values of a region within the rIFC were predictive of its future increase in sulcal depth ($r = 0.28$, $p = 0.005$).

In A- individuals (see Fig. 7B), future thickness changes were predicted by baseline dispersion values in the left IPL ($r = -0.17$, $p = 0.04$), left ACC ($r = -0.18$, $p = 0.03$), right MTG ($r = 0.22$, $p = 0.007$) and right MPFC ($r = -0.22$, $p = 0.009$). Gyrification changes were predicted by baseline dispersion values in the left MTG ($r = 0.18$, $p = 0.03$; $r = 0.20$, $p = 0.01$), left DLPFC ($r = 0.17$, $p = 0.04$) and right MTG ($r = -0.19$, $p = 0.02$). Notably, the right MTG always showed inverted patterns compared with the rest of the significant DMN regions for both thickness and gyrification. Finally, higher baseline dispersion in the left precuneus was associated with increased sulcal depth 2 years later ($r = 0.17$, $p = 0.04$), whereas the left IPL showed an inverted, negative, pattern ($r = -0.17$, $p = 0.04$).

However, none of these correlations survived FDR correction for multiple comparisons.

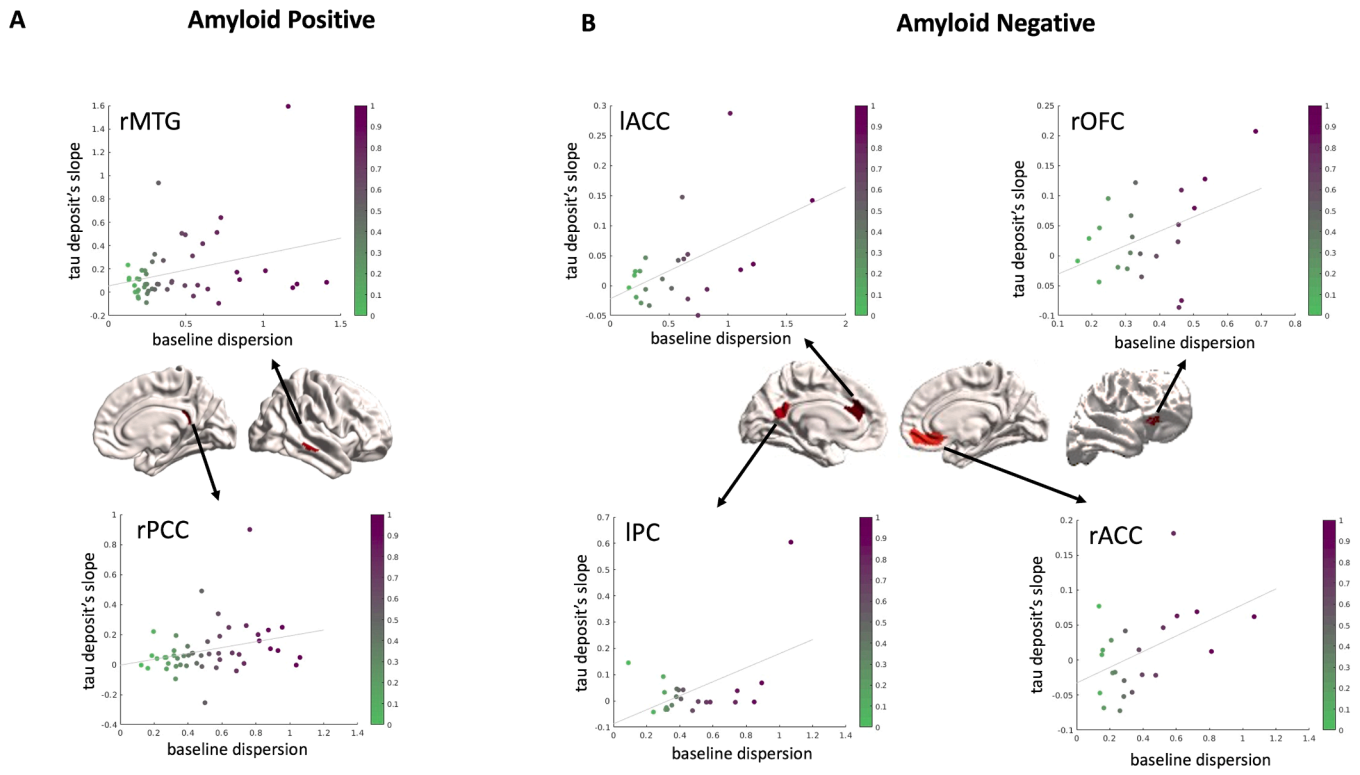

Fig. 6. DMN dispersion values predictive of future tau accumulation. Scatter plots of the DMN regions which dispersion values at baseline were significantly associated with future tau deposits at 2 years follow up for both A+ (**A**) and A- (**B**) individuals. Significant regions are plotted on the surface and color coded based on the directionality of the relationship (i.e., red colors indicate significant positive relationships).
ACC = anterior cingulate cortex, IFC = inferior frontal cortex, *l* = left, MTG = middle temporal gyrus, PCC = posterior cingulate cortex, *r* = right.

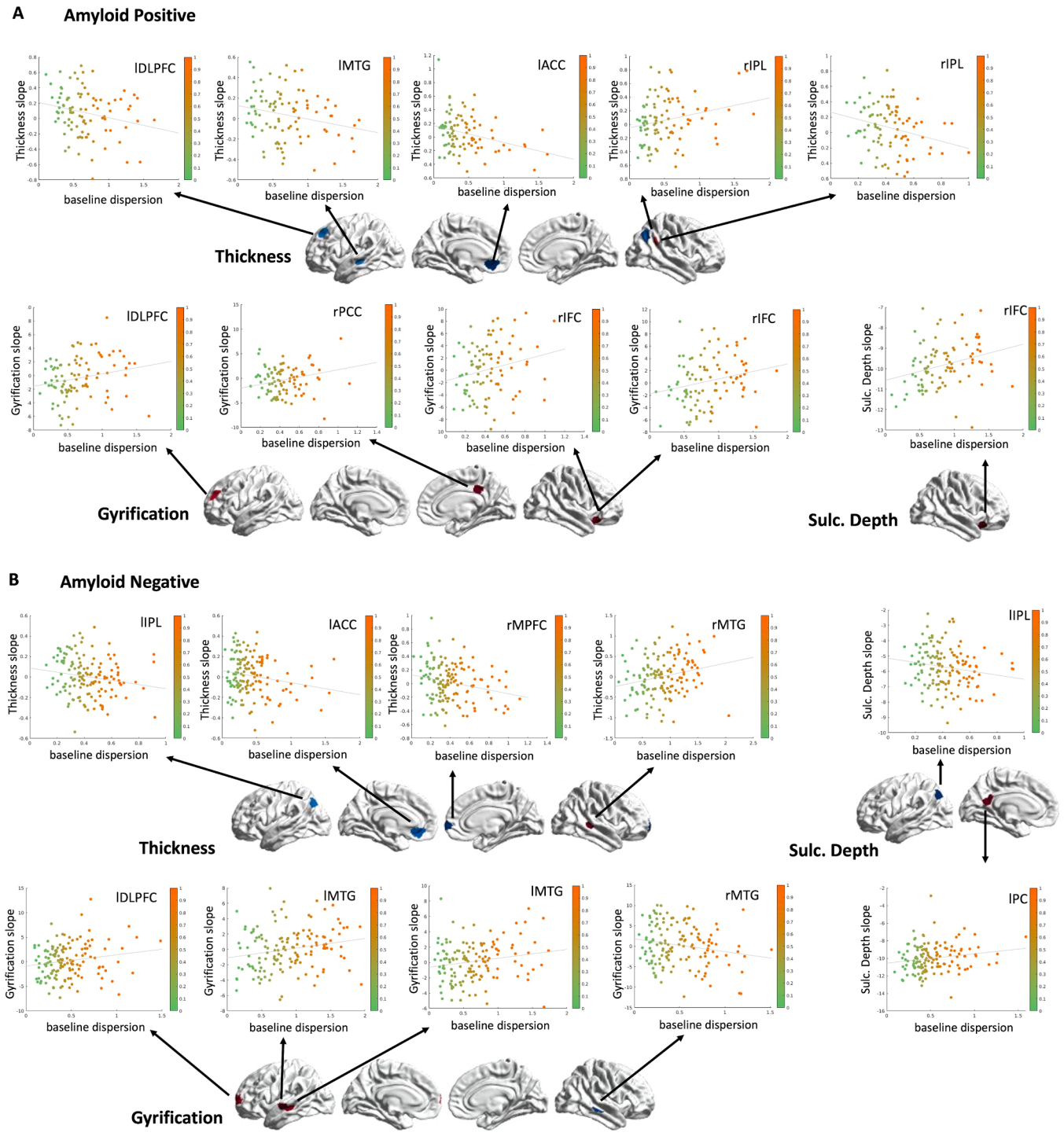

Fig. 7. DMN dispersion values predictive of future structural morphological changes. Scatter plots of the DMN regions in which dispersion values at baseline were significantly associated with future morphological changes (thickness, gyrification and sulcal depth) at 2 years follow up for both *A*+ (**A**) and A- (**B**) individuals. Significant regions are plotted on the surface and color coded based on the directionality of the relationship (i.e., blue colors indicate significant negative relationships whereas positive associations are depicted in red).
ACC = anterior cingulate cortex, DLPFC = dorsolateral prefrontal cortex, IFC = inferior frontal cortex, IPL = inferior parietal lobule, MPFC = medial prefrontal cortex, *l* = left, MTG= middle temporal gyrus, PC = precuneus, PCC = posterior cingulate cortex, *r* = right.

4. Discussion

In this study, we examined DMN gradients' dispersion as a measure of functional decoupling, hypothesizing its relevance as predictor of cognitive performance and clinical severity. Dispersion values were significantly higher in MCI and AD compared with healthy controls and negatively correlated with MMSE scores, aligning with previous findings of progressive DMN disconnection in AD (for a systematic review and meta-analysis, see Badhwar et al., 2017).

Using amyloid status as a diagnostic criterion (Jack et al., 2016), we observed opposite patterns in A+ and A− groups. In line with our expectations, higher dispersion of several DMN regions was negatively associated with behavior, but this was only true in A+ individuals. On the other hand, functional differentiation of the DMN (higher

dispersion) was associated with better memory performance in the A- group. This represents an important difference from our earlier investigation (Menardi et al., 2025), whereby better preserved structural integrity resulted in better memory performance in both A+ and A- individuals and highlights the potentially greater sensitivity of functional measures to the effect of this proteinopathy. It is also relevant for our point to focus on the cohesiveness of the signal within the DMN, arguably the most complex network of the human brain (Mancuso et al., 2022; Margulies et al., 2016; Smallwood et al., 2021). While the DMN benefits from high nodal connectivity between its regions and presents as a single system, its contribution to sustaining a variety of cognitive functions (self-referential thought, social cognition, semantic memory, mental time travel, but also more extrinsic activities) necessarily requires a functional differentiation among its regions (Gordon et al., 2020; Mancuso et al., 2022). In line with the well documented hierarchical and multiscale organization of the brain (Betzel and Bassett, 2017), it is possible to map the heterogeneity within the connectivity patterns of the DMN in discrete subnetworks with differentiable roles in cognitive processing (for a review and meta-analysis, see Mancuso et al., 2022). For instance, up to nine subnetworks have been reliably identified across individuals; these were seen to vary in their role towards internally oriented behavior versus language-related functions (Gordon et al., 2020). Building on this evidence, we argue that, while loss of functional coherence within the network might be pathological and hence exert a negative influence on cognition (here depicted by the negative association between dispersion and memory performance in A+ participants), in healthy individuals (A-) a certain degree of functional differentiation might be indicative of normal DMN heterogeneity. This interpretation is also guided by the observation that significant interactions involved posterior and anterior DMN regions (ACC and DLPFC on one extreme, PCC, precuneus and IPL on the other extreme), where disconnection is more marked in AD patients than in healthy aging (Jones et al., 2011). This result reinforces the idea that a more unitary DMN might be beneficial in pathological scenarios but perhaps less so in healthy individuals. Of note, A+ individuals with high levels of education, a proxy of cognitive reserve, also presented positive associations between dispersion values and memory performance, further corroborating that a certain degree of functional heterogeneity might be linked to a more efficient network.

Temporal regions, however, showed reversed patterns compared with the other DMN regions. For them, greater functional differentiation in the A+ participants was associated with better encoding, retrieval and recall performance. As the temporal cortices are among the first regions displaying tau accumulation and being the spreading of tau driven by functional connectivity (Franzmeier et al., 2020; Ottoy et al., 2024), we argue that the observed positive association with gradients dispersion indicates that diminished connectivity between temporal sites and the rest of the DMN might be beneficial because it limits tau spreading. This is specific to the temporal cortices as tau epicenters, whereas other DMN regions with high levels of tau burden, such as the bilateral ACC, presented the expected negative associations. This phenomenon is in line with the evidence that the reported prion-like spreading of tau is associated with hypoconnectivity between lower and higher tau burden regions (Nabizadeh, 2024), being AD a disconnectome syndrome (Delbeuck et al., 2003). As such, in pathology, functional dispersion is associated with poorer baseline memory performance except for the temporal regions, where it might act as a protective mechanism counteracting tau spreading. This pattern is not observed in A- individuals, given that amyloid acts as an accelerator of tau propagation that would otherwise remain more limited to temporal and cingulate cortices, a condition known as primary age-related tauopathy (PART) (van der Kant et al., 2020). The unique patterns observed in temporal cortices seem specific to their functional decoupling with other regions of the DMN, as this pattern of findings was not observed when solely looking at their degree of structural damage (Menardi et al., 2025).

As for the prediction of future cognitive decline, higher baseline dispersion values were associated with future steeper worsening of memory abilities in both A+ and A- individuals, except for regions presenting high tau burden at baseline. For the latter, we observed that higher functional differentiation (dispersion) at baseline was positively associated with more preserved future memory functions. These regions included the left PCC/precuneus in A+ individuals and the left MTG in A- participants, reflecting the typical spatial patterns of tauopathy as a function of amyloid status (van der Kant et al., 2020).

A series of correlational analyses were also carried out to test the association between regional dispersion and changes in tau burden and morphology, this time without factoring in behavior. First, we observed that higher baseline dispersion was predictive of faster accumulation rates of tau. We believe this is in line with recent evidence on the local effects of connectivity-mediated tau spreading, suggesting that the spreading of tau is accompanied by reduced functional connectivity of non-epicenter tau regions to epicenter tau regions (Nabizadeh, 2024). This generally reflects the progressive distancing of regions in the functional space, representing a clinical hallmark that occurs in aging (Schultz et al., 2017) and becomes more marked in AD (Nabizadeh, 2024). As such, our study presents a dual contribution as it distinguishes in an entirely data-driven fashion between epicenter regions in tau spreading, in which functional dispersion is beneficial to counteract clinical worsening, and non-epicenter regions, in which functional dispersion is linked to worst clinical manifestation in terms of future memory decline and susceptibility to tau accumulation (i.e., the prion-like spreading of tau from epicenter to non-epicenter regions described in Nabizadeh, 2024).

Secondly, we observed that baseline dispersion was a predictor of morphological changes, in terms of future greater thinning and gyrification of the cortex. The former is to be expected as grey matter loss is a hallmark of neurodegeneration, accelerated by AD pathology (Hampton et al., 2020; Roe et al., 2021; Vinke et al., 2018). On the other hand, gyrification tends to decrease during the lifespan (Lamballais et al., 2020), but the speed of such decline slows later in life (Cao et al., 2017). This can result in patterns of increased gyrification both in healthy elderly and AD patients (Cao et al., 2017; Lamballais et al., 2020; Núñez et al., 2020) and has been interpreted as due to white matter atrophy occurring at a faster rate in late adulthood (compared with grey matter) (Lamballais et al., 2020; Vinke et al., 2018), therefore influencing the folding of the cortex.

Finally, as already discussed, greater functional dispersion in the DMN might also reflect a certain degree of healthy heterogeneity in the functional patterns of its regions. In this scenario, the positive association with longitudinal morphological changes might be interpreted as indicative of more preserved structures. This reasoning applies to the changes in sulcal depth observed in the right inferior frontal cortices in the A+ group and in the left precuneus/PCC in the A- individuals. While sulcal depth is expected to decrease with pathology (Im et al., 2008), both regions presented a positive association with baseline dispersion measures, in the form of a reduction in the steepness of the slope (less negative) for those individuals with higher baseline dispersion values. This might reflect a protective mechanism, supported by the observation that, even at baseline, those regions showed a positive association between dispersion values and encoding performance. Not only their functional differentiation is, therefore, linked to better baseline performance, but it is also protective of future structural damage to the same regions.

Finally, we conclude with the observation that those DMN regions in which dispersion was most predictive of baseline memory performance tended to be left lateralized. This can reflect both the verbal nature of the test stimuli, as well as an initial greater vulnerability of the left hemisphere, as already reported in structural and metabolic studies (Jones et al., 2022; Roe et al., 2021; Rubido et al., 2023; Thompson et al., 2001; Zakzanis et al., 2003). The left hemispheric asymmetry was lost at follow-up measurements, possibly due to the advancing of pathology.

A few limitations need to be addressed. For instance, we only

analyzed dispersion measures within the DMN, but future studies are needed to determine if similar patterns are also observed in other resting state networks. Secondly, while we made use of all available ADNI data that met our inclusion criteria, a replication in a different cohort would be desirable. This is especially crucial given that our correlation analyses did not survive FDR correction, probably due to the small sample size. Finally, we observed that dispersion measures showed opposite interactions as a function of amyloid status. However, amyloid accumulation is also found in co-pathology in other neurodegenerative disorders, such as Parkinson's Disease. It would be of value to understand if the results of our study are pathology-specific (thus only observed in AD), or amyloid-determined (possibly present in other neurodegenerative disorders).

In conclusion, our findings reveal a novel and promising role for gradient measures to track pathological breakdown in functional connectivity and its relation to cognitive decline, proteinopathy and atrophy. At the same time, our work also promotes the working hypothesis that a certain degree of functional heterogeneity is key to efficient network processing. Functional dispersion can be seen, therefore, as a useful tool to monitor alterations in a 3D space of its own, in which axes are represented by the healthy-to-pathology continuum, the cognitive performance spectrum and the scattering of region-to-region connectivity from a unitary system.

Authors contributions

Arianna Menardi- Conceptualization, Data curation, Formal analysis, Writing – original draft; Beatrice La Rocca- Data curation, Writing – review & editing; Ceren Saglam- Data curation, Writing – review & editing; Francesco Alberti- Conceptualization, Writing – review & editing; Diego Cecchin- Conceptualization, Writing – review & editing; Annalena Venneri- Conceptualization, Supervision, Writing – review & editing; Annachiara Cagnin- Conceptualization, Supervision, Writing – review & editing; Antonino Vallesi- Conceptualization, Supervision, Writing – review & editing.

Funding

AM is supported by the Associazione Italiana Ricerca Alzheimer Onlus (Airalzh-Grants-for-Young-Reasearchers - AGYR 2023).

AVe is supported by funding obtained under the National Recovery and Resilience Plan (NRRP), Mission 4 Component 2 Investment 1.3—Call for tender No. 341 of 15/03/2022 of the Italian Ministry of University and Research funded by the European Union—NextGenerationEU, Project code PE0000006, Concession Decree No. 1553 of 11/10/2022 adopted by the Italian Ministry of University and Research, CUP D93C22000930002, "A multiscale integrated approach to the study of the nervous system in health and disease" (MNESYS).

Data availability statement

All data used in the analyses are made available in the ADNI's repository (https://ida.loni.usc.edu/login.jsp). Functions used to extract graph theory metrices are available in the Brain Connectivity Toolbox (https://sites.google.com/site/bctnet/); whereas the functions used to extract functional gradients are available in the BrainSpace Toolbox (https://brainspace.readthedocs.io/en/latest/). Measures of gradients' dispersion were computed as described in the work by (Bethlehem et al., 2020) and made available in their repository (https://github.com/rb643/GradientDispersion/tree/master).

CRediT authorship contribution statement

Arianna Menardi: Writing – original draft, Formal analysis, Data curation, Conceptualization. **Beatrice La Rocca:** Writing – review & editing, Data curation. **Ceren Saglam:** Writing – review & editing, Data curation. **Francesco Alberti:** Writing – review & editing, Conceptualization. **Diego Cecchin:** Writing – review & editing, Conceptualization. **Annalena Venneri:** Writing – review & editing, Supervision, Conceptualization. **Annachiara Cagnin:** Writing – review & editing, Supervision, Conceptualization. **Antonino Vallesi:** Writing – review & editing, Supervision, Conceptualization.

Declaration of competing interest

The authors declare that they have no known competing financial interests or personal relationships that could have appeared to influence the work reported in this paper.

Acknowledgements

Data collection and sharing for this project was funded by the Alzheimer's Disease Neuroimaging Initiative (ADNI) (National Institutes of Health Grant U01 AG024904) and DOD ADNI (Department of Defense award number W81XWH-12–2–0012). ADNI is funded by the National Institute on Aging, the National Institute of Biomedical Imaging and Bioengineering, and through generous contributions from the following: AbbVie, Alzheimer's Association; Alzheimer's Drug Discovery Foundation; Araclon Biotech; BioClinica, Inc.; Biogen; Bristol-Myers Squibb Company; CereSpir, Inc.; Cogstate; Eisai Inc.; Elan Pharmaceuticals, Inc.; Eli Lilly and Company; EuroImmun; F. Hoffmann-La Roche Ltd and its affiliated company Genentech, Inc.; Fujirebio; GE Healthcare; IXICO Ltd.; Janssen Alzheimer Immunotherapy Research & Development, LLC.; Johnson & Johnson Pharmaceutical Research & Development LLC.; Lumosity; Lundbeck; Merck & Co., Inc.; Meso Scale Diagnostics, LLC.; NeuroRx Research; Neurotrack Technologies; Novartis Pharmaceuticals Corporation; Pfizer Inc.; Piramal Imaging; Servier; Takeda Pharmaceutical Company; and Transition Therapeutics. The Canadian Institutes of Health Research is providing funds to support ADNI clinical sites in Canada. Private sector contributions are facilitated by the Foundation for the National Institutes of Health (www.fnih.org). The grantee organization is the Northern California Institute for Research and Education, and the study is coordinated by the Alzheimer's Therapeutic Research Institute at the University of Southern California. ADNI data are disseminated by the Laboratory for Neuro Imaging at the University of Southern California.

Supplementary materials

Supplementary material associated with this article can be found, in the online version, at doi:10.1016/j.neuroimage.2026.121696.

References

Alberti, F., Menardi, A., Margulies, D.S., Vallesi, A., 2025. Understanding the link between functional profiles and intelligence through dimensionality reduction and graph analysis. Hum. Brain Mapp. 46, e70149. https://doi.org/10.1002/HBM.70149.

Badhwar, A.P., Tam, A., Dansereau, C., Orban, P., Hoffstaedter, F., Bellec, P., 2017. Resting-state network dysfunction in Alzheimer's disease: a systematic review and meta-analysis. Alzheimer's Dement.: Diagn. Assess. Dis. Monit. 8, 73–85. https://doi.org/10.1016/J.DADM.2017.03.007.

Behzadi, Y., Restom, K., Liau, J., Liu, T.T., 2007. A component based noise correction method (CompCor) for BOLD and perfusion based fMRI. Neuroimage 37, 90. https://doi.org/10.1016/J.NEUROIMAGE.2007.04.042.

Bernhardt, B.C., Smallwood, J., Keilholz, S., Margulies, D.S., 2022. Gradients in brain organization. Neuroimage 251, 118987. https://doi.org/10.1016/J.NEUROIMAGE.2022.118987.

Bethlehem, R.A.I., Paquola, C., Seidlitz, J., Ronan, L., Bernhardt, B., Consortium, C.C.A. N., Tsvetanov, K.A., 2020. Dispersion of functional gradients across the adult lifespan. Neuroimage 222, 117299. https://doi.org/10.1016/J.NEUROIMAGE.2020.117299.

Betzel, R.F., Bassett, D.S., 2017. Multi-scale brain networks. Neuroimage 160, 73–83. https://doi.org/10.1016/J.NEUROIMAGE.2016.11.006.

Braak, H., Braak, E., 1991. Neuropathological stageing of Alzheimer-related changes. Acta Neuropathol. 82, 239–259. https://doi.org/10.1007/BF00308809/METRICS.

Bruno, D., Jauregi-Zinkunegi, A., Bock, J.R., 2024. Predicting CDR status over 36 months with a recall-based digital cognitive biomarker. Alzheimer's Dement. https://doi.org/10.1002/alz.14213.

Buckner, R.L., Snyder, A.Z., Shannon, B.J., LaRossa, G., Sachs, R., Fotenos, A.F., Sheline, Y.I., Klunk, W.E., Mathis, C.A., Morris, J.C., Mintun, M.A., 2005. Molecular, structural, and functional characterization of Alzheimer's disease: evidence for a relationship between default activity, amyloid, and memory. J. Neurosci. 25, 7709–7717. https://doi.org/10.1523/JNEUROSCI.2177-05.2005.

Bullmore, E.T., Bassett, D.S., 2011. Brain graphs: graphical models of the Human Brain connectome. Annu. Rev. Clin. Psychol. 7, 113–140. https://doi.org/10.1146/annurev-clinpsy-040510-143934.

Cao, B., Mwangi, B., Passos, I.C., Wu, M.J., Keser, Z., Zunta-Soares, G.B., Xu, Di., Hasan, K.M., Soares, J.C., 2017. Lifespan gyrification trajectories of Human brain in healthy individuals and patients with major psychiatric disorders. Sci. Rep. 7 (1), 1–8. https://doi.org/10.1038/s41598-017-00582-1, 20177.

Crary, J.F., Trojanowski, J.Q., Schneider, J.A., Abisambra, J.F., Abner, E.L., Alafuzoff, I., Arnold, S.E., Attems, J., Beach, T.G., Bigio, E.H., Cairns, N.J., Dickson, D.W., Gearing, M., Grinberg, L.T., Hof, P.R., Hyman, B.T., Jellinger, K., Jicha, G.A., Kovacs, G.G., Knopman, D.S., Kofler, J., Kukull, W.A., Mackenzie, I.R., Masliah, E., McKee, A., Montine, T.J., Murray, M.E., Neltner, J.H., Santa-Maria, I., Seeley, W.W., Serrano-Pozo, A., Shelanski, M.L., Stein, T., Takao, M., Thal, D.R., Toledo, J.B., Troncoso, J.C., Vonsattel, J.P., White, C.L., Wisniewski, T., Woltjer, R.L., Yamada, M., Nelson, P.T., 2014. Primary age-related tauopathy (PART): a common pathology associated with human aging. Acta Neuropathol. 128, 755–766. https://doi.org/10.1007/S00401-014-1349-0/TABLES/2.

Delbeuck, X., Van Der Linden, M., Collette, F., 2003. Alzheimer's Disease as a disconnection syndrome? Neuropsychol. Rev. 13, 79–92. https://doi.org/10.1023/A:1023832305702/METRICS.

Franzmeier, N., Neitzel, J., Rubinski, A., 2020. Functional brain architecture is associated with the rate of tau accumulation in Alzheimer's disease. Nat. Commun. 11 (1), 1–17. https://doi.org/10.1038/s41467-019-14159-1, 202011.

Gaser, C., Dahnke, R., Thompson, P.M., Kurth, F., Luders, E., 2024. CAT: a computational anatomy toolbox for the analysis of structural MRI data. Gigascience 13, 1–13. https://doi.org/10.1093/GIGASCIENCE/GIAE049.

Gordon, E.M., Laumann, T.O., Marek, S., Raut, R.V., Gratton, C., Newbold, D.J., Greene, D.J., Coalson, R.S., Snyder, A.Z., Schlaggar, B.L., Petersen, S.E., Dosenbach, N.U.F., Nelson, S.M., 2020. Default-mode network streams for coupling to language and control systems. Proc. Natl. Acad. Sci. U.S.A 117, 17308–17319. https://doi.org/10.1073/PNAS.2005238117/SUPPL_FILE/PNAS.2005238117.SAPP.PDF.

Greve, D.N., Fischl, B., 2009. Accurate and robust brain image alignment using boundary-based registration. Neuroimage 48, 63–72. https://doi.org/10.1016/J.NEUROIMAGE.2009.06.060.

Hampton, O.L., Buckley, R.F., Manning, L.K., Scott, M.R., Properzi, M.J., Peña-Gómez, C., Jacobs, H.I.L., Chhatwal, J.P., Johnson, K.A., Sperling, R.A., Schultz, A. P., 2020. Resting-state functional connectivity and amyloid burden influence longitudinal cortical thinning in the default mode network in preclinical Alzheimer's disease. Neuroimage Clin. 28, 102407. https://doi.org/10.1016/J.NICL.2020.102407.

He, Y., Li, Q., Fu, Z., Zeng, D., Han, Y., Li, S., 2023. Functional gradients reveal altered functional segregation in patients with amnestic mild cognitive impairment and Alzheimer's disease. Cereb. Cortex 33, 10836–10847. https://doi.org/10.1093/cercor/bhad328.

Hong, S.J., Xu, T., Nikolaidis, A., Smallwood, J., Margulies, D.S., Bernhardt, B., Vogelstein, J., Milham, M.P., 2020. Toward a connectivity gradient-based framework for reproducible biomarker discovery. Neuroimage 223, 117322. https://doi.org/10.1016/J.NEUROIMAGE.2020.117322.

Hu, Q., Li, Y., Wu, Y., Lin, X., Zhao, X., 2022. Brain network hierarchy reorganization in Alzheimer's disease: a resting-state functional magnetic resonance imaging study. Hum. Brain Mapp. 43, 3498–3507. https://doi.org/10.1002/hbm.25863.

Im, K., Lee, J.M., Won Seo, S., Hyung Kim, S., Kim, S.I., Na, D.L., 2008. Sulcal morphology changes and their relationship with cortical thickness and gyral white matter volume in mild cognitive impairment and Alzheimer's disease. Neuroimage 43, 103–113. https://doi.org/10.1016/j.neuroimage.2008.07.016.

Jack, C.R., Bennett, D.A., Blennow, K., Carrillo, M.C., Dunn, B., Haeberlein, S.B., Holtzman, D.M., Jagust, W., Jessen, F., Karlawish, J., Liu, E., Molinuevo, J.L., Montine, T., Phelps, C., Rankin, K.P., Rowe, C.C., Scheltens, P., Siemers, E., Snyder, H.M., Sperling, R., Elliott, C., Masliah, E., Ryan, L., Silverberg, N., 2018. NIA-AA Research Framework: Toward a biological Definition of Alzheimer's disease. Alzheimer's and Dementia. https://doi.org/10.1016/j.jalz.2018.02.018.

Jack, C.R., Bennett, D.A., Blennow, K., Carrillo, M.C., Feldman, H.H., Frisoni, G.B., Hampel, H., Jagust, W.J., Johnson, K.A., Knopman, D.S., Petersen, R.C., Scheltens, P., Sperling, R.A., Dubois, B., 2016. VIEWS & REVIEWS A/T/N: an unbiased descriptive classification scheme for Alzheimer disease biomarkers.

Jack, C.R., Wiste, H.J., Weigand, S.D., Therneau, T.M., Lowe, V.J., Knopman, D.S., Botha, H., Graff-Radford, J., Jones, D.T., Ferman, T.J., Boeve, B.F., Kantarci, K., Vemuri, P., Mielke, M.M., Whitwell, J., Josephs, K., Schwarz, C.G., Senjem, M.L., Gunter, J.L., Petersen, R.C., 2020. Predicting future rates of tau accumulation on PET. Brain 143, 3136–3150. https://doi.org/10.1093/BRAIN/AWAA248.

Jenkinson, M., Bannister, P., Brady, M., Smith, S., 2002. Improved optimization for the robust and accurate linear registration and motion correction of brain images. Neuroimage 17, 825–841. https://doi.org/10.1006/NIMG.2002.1132.

Jones, D., Lowe, V., Graff-Radford, J., Botha, H., Barnard, L., Wiepert, D., Murphy, M.C., Murray, M., Senjem, M., Gunter, J., Wiste, H., Boeve, B., Knopman, D., Petersen, R., Jack, C., 2022. A computational model of neurodegeneration in Alzheimer's disease. Nat. Commun. 13, 1–13. https://doi.org/10.1038/S41467-022-29047-4.

TECHMETA=57,59,78;SUBJMETA=1283,132,2649,375,378,617,631,692;KWRD=ALZHEIMER.

Jones, D.T., MacHulda, M.M., Vemuri, P., McDade, E.M., Zeng, G., Senjem, M.L., Gunter, J.L., Przybelski, S.A., Avula, R.T., Knopman, D.S., Boeve, B.F., Petersen, R.C., Jack, C.R., 2011. Age-related changes in the default mode network are more advanced in Alzheimer disease. Neurology 77, 1524–1531. https://doi.org/10.1212/WNL.0B013E318233B33D/SUPPL_FILE/APPENDIX_E-1.DOC.

Lamballais, S., Vinke, E.J., Vernooij, M.W., Ikram, M.A., Muetzel, R.L., 2020. Cortical gyrification in relation to age and cognition in older adults. Neuroimage 212, 116637. https://doi.org/10.1016/J.NEUROIMAGE.2020.116637.

Lanctôt, K.L., Hahn-Pedersen, J.H., Eichinger, C.S., Freeman, C., Clark, A., Tarazona, L.R. S., Cummings, J., 2024. Burden of illness in people with Alzheimer's disease: a systematic review of epidemiology, comorbidities mortality. J. Prev. Alzheimers Dis. 11, 97–107. https://doi.org/10.14283/JPAD.2023.61.

Lee, M.D., Bock, J.R., Cushman, I., Shankle, W.R., 2020. An application of multinomial processing tree models and bayesian methods to understanding memory impairment. J. Math. Psychol. 95, 102328. https://doi.org/10.1016/J.JMP.2020.102328.

Mancuso, L., Cavuoti-Cabanillas, S., Liloia, D., Manuello, J., Buzi, G., Cauda, F., Costa, T., 2022. Tasks activating the default mode network map multiple functional systems. Brain Struct. Funct. 227 (5), 1711–1734. https://doi.org/10.1007/S00429-022-02467-0, 2022227.

Margulies, D.S., Ghosh, S.S., Goulas, A., Falkiewicz, M., Huntenburg, J.M., Langs, G., Bezgin, G., Eickhoff, S.B., Castellanos, F.X., Petrides, M., Jefferies, E., Smallwood, J., 2016. Situating the default-mode network along a principal gradient of macroscale cortical organization. Proc. Natl. Acad. Sci. U.S.A 113, 12574–12579. https://doi.org/10.1073/PNAS.1608282113/SUPPL_FILE/PNAS.201608282SI.PDF.

Menardi, A., Saglam, C., La Rocca, B., Cecchin, D., Venneri, A., Cagnin, A., Vallesi, A., 2025. Cortical morphology changes in default mode network regions as predictors of cognitive decline in relation to amyloid and tau deposits. Brain Commun. https://doi.org/10.1093/BRAINCOMMS/FCAF320.

Menardi, A., Spoa, M., Vallesi, A., 2024. Brain topology underlying executive functions across the lifespan: focus on the default mode network. Front. Psychol. 15, 1441584. https://doi.org/10.3389/FPSYG.2024.1441584/PDF.

Menon, V., 2023. 20 years of the default mode network: a review and synthesis. Neuron 111, 2469–2487. https://doi.org/10.1016/j.neuron.2023.04.023.

Nabizadeh, F., 2024. Disruption in functional networks mediated tau spreading in Alzheimer's disease. Brain Commun. 6. https://doi.org/10.1093/BRAINCOMMS/FCAE198.

Nandi, A., Counts, N., Chen, S., Seligman, B., Tortorice, D., Vigo, D., Bloom, D.E., 2022. Global and regional projections of the economic burden of Alzheimer's disease and related dementias from 2019 to 2050: a value of statistical life approach. EClinicalMedicine 51, 101580. https://doi.org/10.1016/j.eclinm.2022.101580.

Nieto-Castanon, A., 2020. FMRI denoising pipeline. Handbook of functional connectivity magnetic resonance imaging methods in CONN 17–25. https://doi.org/10.56441/HILBERTPRESS.2207.6600.

Núñez, C., Callén, A., Lombardini, F., Compta, Y., Stephan-Otto, C., 2020. Different cortical gyrification patterns in Alzheimer's Disease and impact on memory performance. Ann. Neurol. 88, 67–80. https://doi.org/10.1002/ANA.25741.

Ottoy, J., Kang, M.S., Tan, J.X.M., Boone, L., Vos de Wael, R., Park, B.Y., Bezgin, G., Lussier, F.Z., Pascoal, T.A., Rahmouni, N., Stevenson, J., Fernandez Arias, J., Therriault, J., Hong, S.J., Stefanovic, B., McLaurin, J.A., Soucy, J.P., Gauthier, S., Bernhardt, B.C., Black, S.E., Rosa-Neto, P., Goubran, M., 2024. Tau follows principal axes of functional and structural brain organization in Alzheimer's disease. Nat. Commun. 15 (1), 1–18. https://doi.org/10.1038/s41467-024-49300-2, 202415.

Palmqvist, S., Schöll, M., Strandberg, O., Mattsson, N., Stomrud, E., Zetterberg, H., Blennow, K., Landau, S., Jagust, W., Hansson, O., 2017. Earliest accumulation of β-amyloid occurs within the default-mode network and concurrently affects brain connectivity. Nat. Commun. 8 (1), 1–13. https://doi.org/10.1038/s41467-017-01150-x, 20178.

Perovnik, M., Tang, C.C., Namías, M., Eidelberg, D., 2023. Longitudinal changes in metabolic network activity in early Alzheimer's disease. Alzheimer's Dement. 19, 4061–4072. https://doi.org/10.1002/ALZ.13137.

Roe, J.M., Vidal-Piñeiro, D., Sørensen, Ø., Brandmaier, A.M., Düzel, S., Gonzalez, H.A., Kievit, R.A., Knights, E., Kühn, S., Lindenberger, U., Mowinckel, A.M., Nyberg, L., Park, D.C., Pudas, S., Rundle, M.M., Walhovd, K.B., Fjell, A.M., Westerhausen, R., Masters, C.L., Bush, A.I., Fowler, C., Darby, D., Pertile, K., Restrepo, C., Roberts, B., Robertson, J., Rumble, R., Ryan, T., Collins, S., Thai, C., Trounson, B., Lennon, K., Li, Q.X., Ugarte, F.Y., Volitakis, I., Vovos, M., Williams, R., Baker, J., Russell, A., Peretti, M., Milicic, L., Lim, L., Rodrigues, M., Taddei, K., Taddei, T., Hone, E., Lim, F., Fernandez, S., Rainey-Smith, S., Pedrini, S., Martins, R., Doecke, J., Bourgeat, P., Fripp, J., Gibson, S., Leroux, H., Hanson, D., Dore, V., Zhang, P., Burnham, S., Rowe, C.C., Villemagne, V.L., Yates, P., Pejoska, S.B., Jones, G., Ames, D., Cyarto, E., Lautenschlager, N., Barnham, K., Cheng, L., Hill, A., Killeen, N., Maruff, P., Silbert, B., Brown, B., Sohrabi, H., Savage, G., Vacher, M., 2021. Asymmetric thinning of the cerebral cortex across the adult lifespan is accelerated in Alzheimer's disease. Nat. Commun. 12 (1), 1–11. https://doi.org/10.1038/s41467-021-21057-y, 202112.

Rubido, N., Riedel, G., Vuksanović, V.V., Vuksanović, Vesna, Vuksanović, Vuksanović, 2023. Genetic basis of anatomical asymmetry and aberrant dynamic functional networks in Alzheimer's disease. Brain Commun. 6. https://doi.org/10.1093/BRAINCOMMS/FCAD320.

Rubinov, M., Kötter, R., Hagmann, P., Sporns, O., 2009. Brain connectivity toolbox: a collection of complex network measurements and brain connectivity datasets. Neuroimage 47, S169. https://doi.org/10.1016/S1053-8119(09)71822-1.

Rubinov, M., Sporns, O., 2010. Complex network measures of brain connectivity: uses and interpretations. Neuroimage 52, 1059–1069. https://doi.org/10.1016/J.NEUROIMAGE.2009.10.003.

Schaefer, A., Kong, R., Gordon, E.M., Laumann, T.O., Zuo, X.-N., Holmes, A.J., Eickhoff, S.B., Yeo, B.T.T., 2018. Local-global parcellation of the Human cerebral cortex from intrinsic functional connectivity MRI. Cereb. Cortex 28, 3095–3114. https://doi.org/10.1093/CERCOR/BHX179.

Schuff, N., Woerner, N., Boreta, L., Kornfield, T., Shaw, L.M., Trojanowski, J.Q., Thompson, P.M., Jack, C.R., Weiner, M.W., 2009. MRI of hippocampal volume loss in early Alzheimer's disease in relation to ApoE genotype and biomarkers. Brain 132, 1067–1077. https://doi.org/10.1093/BRAIN/AWP007.

Schultz, A.P., Chhatwal, J.P., Hedden, T., Mormino, E.C., Hanseeuw, B.J., Sepulcre, J., Huijbers, W., LaPoint, M., Buckley, R.F., Johnson, K.A., Sperling, R.A., 2017. Phases of hyperconnectivity and hypoconnectivity in the default mode and salience networks track with amyloid and tau in clinically normal individuals. J. Neurosci. 37, 4323–4331. https://doi.org/10.1523/JNEUROSCI.3263-16.2017.

Smallwood, J., Bernhardt, B.C., Leech, R., Bzdok, D., Jefferies, E., Margulies, D.S., 2021. The default mode network in cognition: a topographical perspective. Nat. Rev. Neurosci. 22 (8), 503–513. https://doi.org/10.1038/s41583-021-00474-4, 202122.

Talwar, P., Kushwaha, S., Chaturvedi, M., Mahajan, V., 2021. Systematic review of different neuroimaging correlates in mild cognitive impairment and Alzheimer's disease. Clin. Neuroradiol. 31, 953–967. https://doi.org/10.1007/S00062-021-01057-7/TABLES/2.

Tarawneh, R., Holtzman, D.M., 2012. The clinical problem of symptomatic Alzheimer disease and mild cognitive impairment. Cold Spring Harb. Perspect. Med. 2, a006148. https://doi.org/10.1101/CSHPERSPECT.A006148.

Thompson, P.M., Mega, M.S., Woods, R.P., Zoumalan, C.I., Lindshield, C.J., Blanton, R. E., Moussai, J., Holmes, C.J., Cummings, J.L., Toga, A.W., 2001. Cortical change in Alzheimer's disease detected with a disease-specific population-based brain atlas. Cereb. Cortex 11, 1–16. https://doi.org/10.1093/CERCOR/11.1.1.

Tustison, N.J., Cook, P.A., Holbrook, A.J., Johnson, H.J., Muschelli, J., Devenyi, G.A., Duda, J.T., Das, S.R., Cullen, N.C., Gillen, D.L., Yassa, M.A., Stone, J.R., Gee, J.C., Avants, B.B., 2021. The ANTsX ecosystem for quantitative biological and medical imaging. Sci. Rep. 11 (1), 1–13. https://doi.org/10.1038/s41598-021-87564-6, 202111.

van der Kant, R., Goldstein, L.S.B., Ossenkoppele, R., 2020. Amyloid-β-independent regulators of tau pathology in Alzheimer disease. Nat. Rev. Neurosci. 21, 21–35. https://doi.org/10.1038/S41583-019-0240-3.

Veréb, D., Mijalkov, M., Chang, Y.W., Canal-Garcia, A., Gomez-Ruis, E., Maass, A., Villeneuve, S., Volpe, G., Pereira, J.B., 2023. Functional gradients of the medial parietal cortex in a healthy cohort with family history of sporadic Alzheimer's disease. Alzheimers. Res. Ther. 15, 1–13. https://doi.org/10.1186/S13195-023-01228-3/FIGURES/5.

Vinke, E.J., de Groot, M., Venkatraghavan, V., Klein, S., Niessen, W.J., Ikram, M.A., Vernooij, M.W., 2018. Trajectories of imaging markers in brain aging: the Rotterdam Study. Neurobiol. Aging 71, 32–40. https://doi.org/10.1016/J.NEUROBIOLAGING.2018.07.001.

Vos de Wael, R., Benkarim, O., Paquola, C., Lariviere, S., Royer, J., Tavakol, S., Xu, T., Hong, S.J., Langs, G., Valk, S., Misic, B., Milham, M., Margulies, D., Smallwood, J., Bernhardt, B.C., 2020. BrainSpace: a toolbox for the analysis of macroscale gradients in neuroimaging and connectomics datasets. Commun. Biol. 3 (1), 1–10. https://doi.org/10.1038/s42003-020-0794-7, 20203.

Wang, D., Li, Z., Zhao, K., Chen, P., Yang, F., Yao, H., Zhou, B., Wei, Y., Lu, J., Chen, Y., Zhang, X., Han, Y., Wang, P., Liu, Y., 2024a. Macroscale gradient dysfunction in Alzheimer's disease: patterns with cognition terms and gene expression profiles. Hum. Brain Mapp. 45, e70046. https://doi.org/10.1002/hbm.70046.

Wang, Y., Li, Q., Yao, L., He, N., Tang, Y., Chen, L., Long, F., Chen, Y., Kemp, G.J., Lui, S., Li, F., 2024b. Shared and differing functional connectivity abnormalities of the default mode network in mild cognitive impairment and Alzheimer's disease. Cereb. Cortex 34. https://doi.org/10.1093/CERCOR/BHAE094.

Whitwell, J.L., Martin, P., Graff-Radford, J., Machulda, M.M., Senjem, M.L., Schwarz, C. G., Weigand, S.D., Spychalla, A.J., Drubach, D.A., Jack, C.R., Lowe, V.J., Josephs, K. A., 2019. The role of age on tau PET uptake and gray matter atrophy in atypical Alzheimer's disease. Alzheimer's Dement. 15, 675–685. https://doi.org/10.1016/J.JALZ.2018.12.016.

Yu, M., Sporns, O., Saykin, A.J., 2021. The human connectome in Alzheimer disease — Relationship to biomarkers and genetics. Nat. Rev. Neurol. 17 (9), 545–563. https://doi.org/10.1038/s41582-021-00529-1, 202117.

Zakzanis, K.K., Graham, S.J., Campbell, Z., 2003. A meta-analysis of structural and functional brain imaging in dementia of the Alzheimer's type: a neuroimaging profile. Neuropsychol. Rev. 13, 1–18. https://doi.org/10.1023/A:1022318921994/METRICS.

Zhang, Y., Brady, M., Smith, S., 2001. Segmentation of brain MR images through a hidden Markov random field model and the expectation-maximization algorithm. IEEe Trans. Med. ImAging 20, 45–57. https://doi.org/10.1109/42.906424.

Zhou, B., Dou, X., Wang, W., Yao, H., Feng, F., Wang, P., Yang, Z., An, N., Liu, B., Zhang, X., Liu, Y., 2022. Structural and functional connectivity abnormalities of the default mode network in patients with Alzheimer's disease and mild cognitive impairment within two independent datasets. Methods 205, 29–38. https://doi.org/10.1016/j.ymeth.2022.06.001.